HEAT TRANSPORT IN MAGNETOHYDRODYNAMIC DUCT FLOW REGIMES WITH CONDUCTING AND INSULATING WALLS

Andreu Queralt
Institut für Thermo- und Fluiddynamik
TU Ilmenau
P.O.Box 100565, D-98684 Ilmenau
andreu.queralt-mcbride@tu-ilmenau.de

Dmitry Krasnov
Institut für Thermo- und Fluiddynamik
TU Ilmenau
P.O.Box 100565, D-98684 Ilmenau
dmitry.krasnov@tu-ilmenau.de

Yuri Kolesnikov
Institut für Thermo- und Fluiddynamik
TU Ilmenau
P.O.Box 100565, D-98684 Ilmenau
yuri.kolesnikov@tu-ilmenau.de

Jörg Schumacher
Institut für Thermo- und Fluiddynamik
TU Ilmenau
P.O.Box 100565, D-98684 Ilmenau
joerg.schumacher@tu-ilmenau.de

ABSTRACT

The flow of a liquid metal (LM) in a rectangular duct segment, subject to a uniform transverse magnetic field and uniform heating at the side walls is explored in an ample parameter space using Direct Numerical Simulation (DNS). We modify electrical wall conductivity, (either highly conducting or perfectly insulating) and investigate the effects of the buoyancy force, both in horizontally and vertically orientated ducts. In the latter case, it may be directed either with the flow or against the flow, creating backflow regions. In this parameter space and with the presence of vortex promoters at the inlet of the duct we identify 4 types of flow. We calculate the Nusselt number $Nu(t)$ for each of them and study the statistical properties to compare their heat transfer capabilities in future fusion reactor blankets.

INTRODUCTION

One of the main candidates for coolant in future fusion reactors are liquid metals which flow inside the blankets. They satisfy operational requirements and, due to the flow of neutrons from the plasma core, tritium breeding can occur to provide fuel for future reactions. Despite these advantages, several engineering questions regarding their viability are still open. In the TOKAMAK context, the flow is subject to strong magnetic fields. The toroidal field component in particular is present in the blanket. Depending on the orientation of the duct, this component will be either in the streamwise direction or along two of the side walls. A second, smaller component is present in the poloidal direction of the TOKAMAK. For simplicity we will consider only the toroidal field, which will be perpendicular to the streamwise direction.

In the case of conducting duct walls, the Lorenz force increases, dampens the velocity and increases the pressure drop ΔP needed to pump the metal with sufficient volume flux (Molokov *et al.*, 2007). Additionally, an M-profile is formed at the Shercliff layers. The strong velocity gradients at the walls are detrimental, both to the production of tritium and the lifespan of the duct, with the steep velocity gradients increasing corrosion at the walls (Smolentsev *et al.*, 2013).

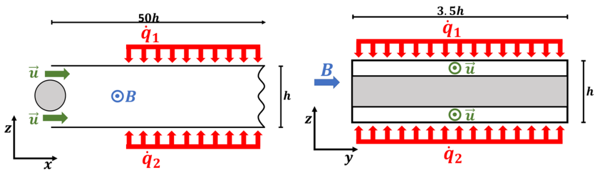

Figure 1. Simulated setup schematic for the duct. Left: side view. Right: downstream view.

To overcome these problems, ceramic Flow Channel Inserts (FCI) are mounted at the duct walls. These come with their own set of problems, such as different heat dilatation from the metal, development of cracks and disintegration under the neutron flux, the latter of which increases maintenance requirements (see, e.g., Smolentsev (2021) for an overview).

DUCT GEOMETRY

Figure 1 shows the simulation domain, a rectangular duct of aspect ratio $L_y/h = 3.5$ is considered. To maintain cohesion with previous studies, such as in Krasnov *et al.* (2023*b*), the length of the duct L_x is 50 times its height h and at the inlet we also prescribe a velocity profile with two flat jets near the top and bottom walls. This profile mimics the velocity field past a round cylinder, which was used in experiments (Krasnov *et al.*, 2023*b*) to generate inlet instabilities by covering $\sim 50\%$ of the inlet area (see figure 1). When heating is applied it is done only at the Shercliff walls, while the Hartmann walls remain adiabatic. Both Shercliff walls are heated to simplify the problem by imposing symmetry. The heating area begins at $x = 20$, again to maintain cohesion with previous studies. When the conductivity of the wall is present, it is set equal at all four walls.

MATHEMATICAL MODEL

In order to solve the flow of the liquid metal, the governing equations are used for an incompressible flow at low magnetic Reynolds numbers Rm, known as quasi-static approximation (see, e.g., Davidson (2016)):

$$\nabla \cdot \boldsymbol{u} = 0 \tag{1}$$

$$\frac{\partial \boldsymbol{u}}{\partial t} + (\boldsymbol{u} \cdot \nabla)\boldsymbol{u} = -\nabla p + \frac{1}{Re}\left(\nabla^2 \boldsymbol{u} + Ha^2 \boldsymbol{j} \times \boldsymbol{e}_B\right) - \frac{Gr}{Re^2} T \boldsymbol{e}_g \tag{2}$$

$$\frac{\partial T}{\partial t} + \boldsymbol{u} \cdot \nabla T = \frac{1}{RePr} \nabla^2 T \tag{3}$$

$$\boldsymbol{j} = -\nabla \phi + \boldsymbol{u} \times \boldsymbol{e}_B \tag{4}$$

$$\nabla^2 \phi = \nabla \cdot (\boldsymbol{u} \times \boldsymbol{e}_B) \tag{5}$$

Here $\boldsymbol{u}$, p, T, $\boldsymbol{j}$ and ϕ are the velocity, pressure, temperature, current density and electric potential fields. For conducting cases, we use the thin wall approximation (see Krasnov *et al.* (2023*a*) and references therein). This model assumes that the currents close within the (thin) walls. Non-dimensional parameters Re, Ha, Pr and Gr are the Reynolds, Hartmann, Prandtl and Grashof numbers respectively, defined as $Re = U_0 L/\nu$, $Ha = BL(\sigma/\rho\nu)^{1/2}$, $Pr = \nu k^{-1}$, $Gr = g\beta q_w L^4/\lambda \nu^2$. The half-height of the duct $L = h/2$ and the mean velocity U_0 in the streamwise direction are used as the length and velocity scales. Finally, $\boldsymbol{e}_g$ and $\boldsymbol{e}_B$ are the unit vectors in the directions of acceleration due to gravity and the imposed magnetic field. The equations are solved numerically using our in-house finite-difference solver described in (Krasnov *et al.* (2023*a*)).

THE NUSSELT NUMBER

To compare the heat transfer efficiency of the different flow regimes, we will use the Nusselt number Nu, defined as (Bejan, 2004):

$$Nu(x,t) = \frac{q' L}{k(T_w(x,t) - T_b(x,t))} \tag{6}$$

Where $q'$is the heat flux across the duct wall, L the duct half-height, k the thermal conductivity, T_b the bulk temperature and T_w the wall temperature. For our simulations, we computed $Nu(x,t)$ using both the top and bottom walls and found that the results were similar, for the insulating duct runs the most notable difference was with a 180 phase shift between them. For the conducting duct, the phase difference was not constant. Figure 2 shows an example of $Nu(x,t)$ where this is clearly visible. The average $Nu(x,t)$ along the duct length is calculated with equation 7. Where l_0 is the starting position for heating and l_f is the duct length. Due to the imposed symmetry of the problem, this value is statistically the same when measured from both walls.

$$Nu(t) = \int_{l_0}^{l_f} Nu(x,t) dx \tag{7}$$

For the remainder of the paper, we take $Nu(t)$ to be the duct-averaged $Nu(t)$ at the top wall ($z = +h/2$). In addition, $\overline{Nu}$ will be the time average of $Nu(t)$:

$$\overline{Nu} = \int_{t_0}^{t_f} Nu(t) dt, \tag{8}$$

where t_0 is taken once the flow is fully developed. For our case, we take $t_0 = 200$ convective time units, which is the longest initial transient we encountered (see *QM* flow in figure 9). The end point of our simulations is $t_f = 600$ in convective units.

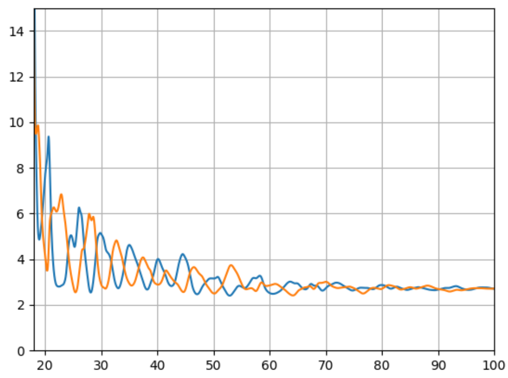

Figure 2. $Nu(x)$ at the top and bottom walls for $Re = 4000$, $Ha = 325$ $c_W = 0$ and passive heat transport

SIMULATION PARAMETERS

Table 1 shows the parameters used for the simulations performed for this paper. We also performed simulations with $c_W = 0.1$ with upward and downward flows and did not see any noticeable effect. The simulations were also performed at $Ha = 500, 750$, however, the results are not shown in this paper. To evaluate the efficiency of the vortex promoters, we also performed simulations with laminar flow at the inlet, but only for the duct in a horizontal position. All simulations were run on a $4096 \times 320 \times 92$ grid with uniform meshing in the streamwise x-direction and strong clustering towards the walls in the y- and z-directions.

THE FOUR FLOW TYPES

We classify the flow regimes into four categories. Figure 3 shows the parameters at which each flow type has been encountered.

1. UL-Flow: Statistically stationary Unstable Walker flow with M-Profile between the Shercliff walls.
2. *QH*-Flow: Statistically stationary quasi-2D (*Q2D*) rolls. These rolls eventually decay into a Hartmann flow.
3. *QW*-Flow: Intermittent *Q2D* rolls with backflow jets (W shape) at the Shercliff layers.
4. *QM*-Flow: Intermittent *Q2D* rolls with side jets at the Shercliff layers (M shape, but weaker than in the UL flow)

The first type of flow occurs when the duct walls are highly conducting. All other types of flow occur with perfectly insulating ducts. The intermittent regimes occur when the duct is in a vertical position. In those situations, the buoyancy force is large enough to modify the velocity profile at the Shercliff layers, where the current is parallel to the magnetic field and thus the Lorenz force is zero. At the bulk and Hartman layers, the buoyancy force acts to modify the velocity magnitude, but since the Lorenz force is proportional to it, the effects are neutralized. This creates either an M-shaped (when the mean flow is directed upwards) or a W-shaped profile (when the mean flow is directed downwards) at the side walls. Eventually velocity gradients become large enough to trigger instabilities, which eventually die out and the original state is restored.

For the case of perfectly insulating walls with $c_W = 0$ at higher Ha, there is a lengthy transient before the flow reaches its final state. Initially, two vortex streaks appear instead of one. In both vertical duct orientations, these streaks eventually

Simulation	Re	Ha	Pr	Gr	c_W	Flow Direction	Observed Flow
1	4000	325	0.02	10^6	0.0	Horizontal	QH
2	4000	325	0.02	10^6	0.1	Horizontal	UL
3	4000	325	0.02	10^6	0.0	Upwards	QM
4	4000	325	0.02	10^6	0.0	Downwards	QW
5	4000	1000	0.02	10^6	0.0	Horizontal	QH
6	4000	1000	0.02	10^6	0.1	Horizontal	UL
7	4000	1000	0.02	10^6	0.0	Upwards	QM
8	4000	1000	0.02	10^6	0.0	Downwards	QW

Table 1. Simulation parameters and observed flow type.

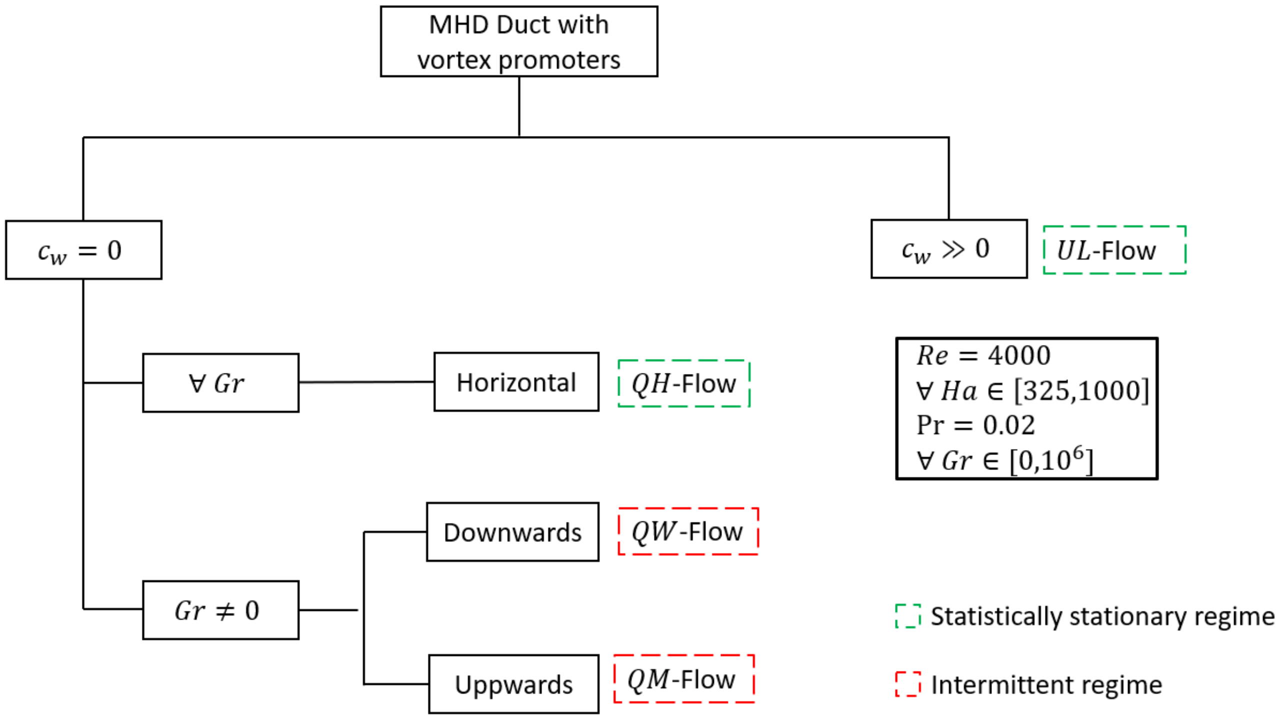

Figure 3. Schematic overview of the parameters at which each flow type exist.

become just one. In the horizontal duct, the flow linearizes, and after some time develops a single streak.

In highly conducting ducts, the Shercliff sidewall jets develop instabilities known as jet-detachments, often found even at low-Re regimes (Braiden *et al.*, 2016). These detachments can be triggered either by the inlet vortex promoters or naturally, due to the strong velocity gradients with inflection points (Priede *et al.*, 2010; Arlt *et al.*, 2017), formed between the Shercliff layers. This, once again, is observed at the higher values of Ha.

In this study, we focus on results at $Ha = 325$ and 1000, which are the lowest and highest values that we have considered. Figure 4 shows instantaneous snapshots for each of the flow types at $Ha = 325$.

RESULTS

Table 2 shows the time averaged Nu numbers and their standard deviation for all four regimes at $Ha = 325$ and $Ha = 1000$ in the presence of vortex promoters. Table 3 shows the same for the horizontal flow in the absence of vortex promoters. Together with figure 5 they provide a birds eye view of the dependence of $\overline{Nu}$ and its time fluctuations with Ha and the flow type. In general, $\overline{Nu}$ Increases with Ha, with the exception of the QW floe, in which Nu decreases significantly. This regime also has the highest variance. In both cases, the highest Nu was observed by the UL flow. At $Ha = 1000$ the vortex promoters have no effect, since the disturbances occur naturally. At $Ha = 325$, however, the flow is laminar without the promoters. Despite this, the Nu is still higher than for all three insulating wall cases at $Ha = 325$, which are very similar to each other. This is because in the UL flow as a fluid parcel is heated by conduction from the walls, it is quickly advected downstream by the high-speed sidewall jets. This results in lower fluid temperatures close to the walls, which reduces the temperature gradient between the walls and the bulk, resulting in higher Nu. At higher Ha, the side jets of the QM flow become more pronounced, so this flow type ends with a better

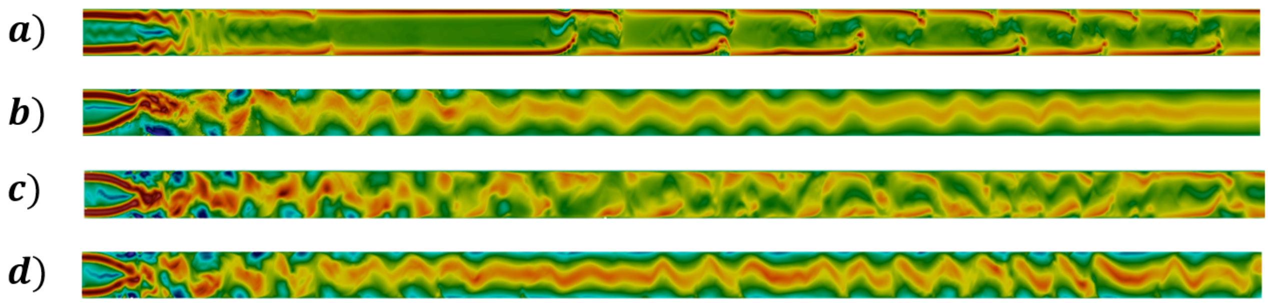

Figure 4. $M-$profile with detachments in the Shercliff layers in a conducting duct$a$), $Q2D$ rolls in a perfectly insulating horizontal duct b), upwards-flow duct with buoyancy driven side wall jets c) and downwards-flow duct with buoyancy driven backflow side wall jets d) All four are at $Re = 4000$, $Ha = 325$, $Gr = 10^6$ and $Pr = 0.02$. $c_W = 0.1$. at a) and $c_W = 0.0$ at b), c) and d)

	$Ha = 325$		$Ha = 1000$	
Flow Type	$\overline{Nu}$	std($\overline{Nu}$)	$\overline{Nu}$	std($\overline{Nu}$)
Q	3.88	0.138	4.07	0.0508
UL	5.36	0.138	6.43	0.041
QM	4.09	0.152	4.65	0.090
QW	4.08	0.411	2.61	0.303

Table 2. Time-averaged Nu for the entire duct length and their standard deviation for $Re = 4000$, $Gr = 10^6$, $Pr = 0.02$ at $Ha = 325$ and $Ha = 1000$. Simulations with vortex promoters

	$Ha = 325$		$Ha = 1000$	
c_W	$\overline{Nu}$	std($\overline{Nu}$)	$\overline{Nu}$	std($\overline{Nu}$)
0.0	3.27	0.0465	3.80	0.0434
0.1	4.68	$3.65 \cdot 10^{-5}$	6.44	0.356

Table 3. Time-averaged Nu for the entire duct length. And their standard deviation for $Re = 4000$, $Gr = 10^6$, $Pr = 0.02$ at $Ha = 325$ and $Ha = 1000$. Base case without vortex promoters

Nu than the QH and QW flows.

Figures 6 and 7 show the time evolution of $\overline{Nu}$, and figures 8 and 9 show the TKE of the same flows. The QW flow, which has poor Nu-performance has the highest TKE, followed by the QM flow, indicating that those are better at mixing. This is because the same fluid parcel that was quickly advected out of the duct in the UL flow is advected not only in the stream wise direction but also strongly in the vertical direction. This causes the heat from the neutron flux to remain longer in the duct, and therefore higher temperatures, specially close to the wall and a lower $\overline{Nu}$

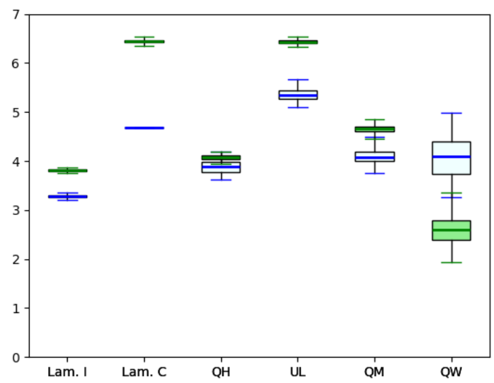

Figure 5. Box plots of $\overline{Nu}$ without vortex promoters with insulating walls (Laminar I), conducting walls (Laminar C) and each of the four regimes encountered with vortex promoters at $Ha = 325$ (blue) and $Ha = 1000$. Outliers have been remove from the plot to avoid cluttering.

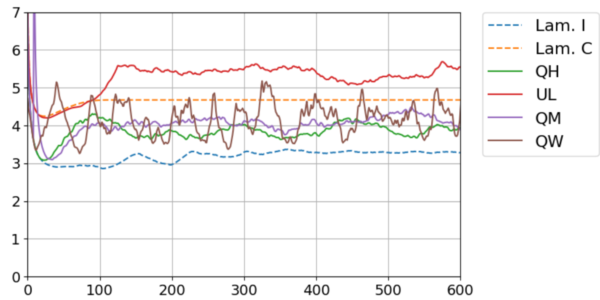

Figure 6. Temporal evolution of $\overline{Nu}$ for the four flow types over 600 convective time units at $Ha = 325$, including initial transient. Dashed lines represent simulations without vortex promoters

DISCUSSION

The results presented here lead to a seemingly non-straightforward conclusion. Namely, for the parameter space that we considered, it turns out that good heat transfer regimes are poor mixing regimes and vice-versa.

From a purely thermodynamic point of view, the best configuration for the LM blanket is the conducting duct, regardless of orientation. However, the same side jets that provide optimal heat transfer are also responsible for the high velocity gradients that can cause corrosion and poor neutron breeding, as well as an unacceptable MHD pressure drop. An alternative, is to leverage the QM flow, which also has side jets, albeit much weaker ones. Figure 11 shows the magnitude of the jets of the UL and QM flows, and figure 12 their gradients in symmetric logarithmic scale. The strongest gradient is one order of magnitude smaller in the QM flow than it is in the UL flow,

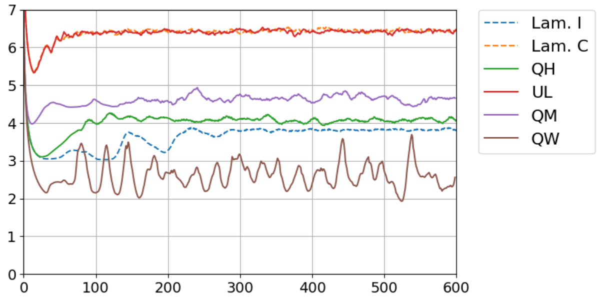

Figure 7. Temporal evolution of $\overline{Nu}$ for the four flow types over 600 convective time units at $Ha = 1000$, including initial transient

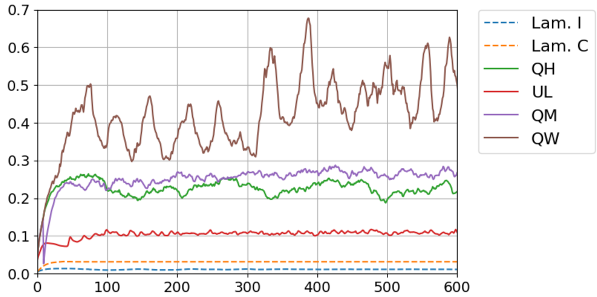

Figure 8. Temporal evolution of the volume averaged duct TKE for 600 convective time units at $Ha = 325$, including initial transient. Dashed lines represent simulations without vortex promoters

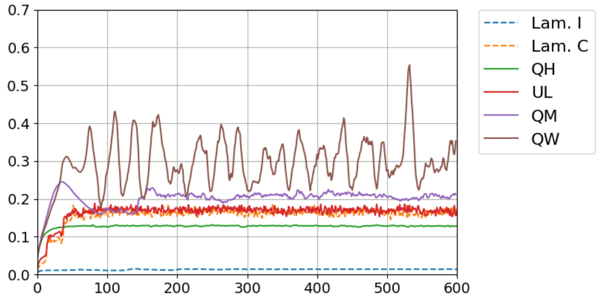

Figure 9. Temporal evolution of the volume averaged duct TKE for 600 convective time units at $Ha = 1000$, including initial transient

while the reduction of Nu is only of about 30%. Figure 10 shows a proposal for how the LM could be pumped in a blanket. If the pumping direction is upwards, then side jets will be present regardless of the wall conductivity. Then, as it returns downwards the liquid metal is fully mixed.

The matter of making the duct walls fully insulating however also leads to engineering problems (Smolentsev, 2021). That is, the neutron flux is known to destroy the FCI used to ensure the ducts are insulating. We have conducted preliminary simulations which suggest that by insulating only the Hartmann walls, which are not exposed to the neutron flux, the resulting flow is the same as for the fully insulating case. This is because more electric current lines are allowed to close inside the duct, compared to insulating all four walls, which appears to be sufficient to reduce the net Lorenz force and the associated MHD pressure drop.

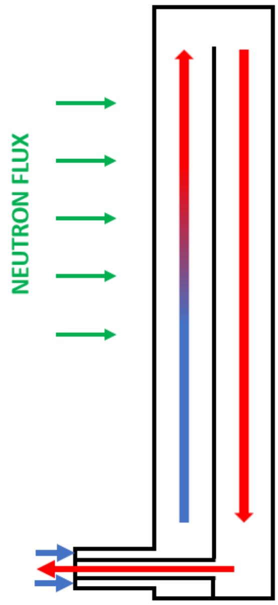

Figure 10. Possible blanket configuration with fluid in the neutron-facing wall being pumped upwards and the flowing back downwards, ensuring best possible mixing.

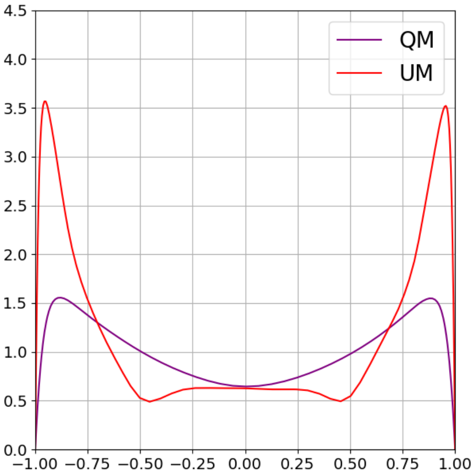

Figure 11. Time averaged velocity over 200 convective time units between the Shercliff layers at $x = 100$ for the UL and QM flow regimes

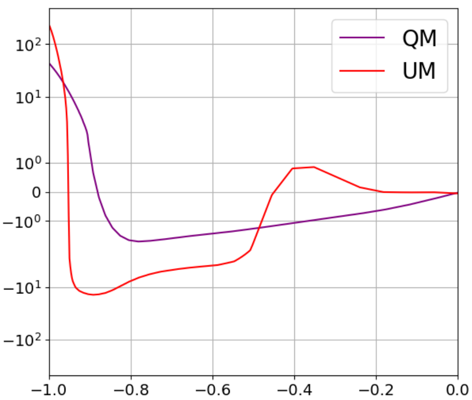

Figure 12. Time averaged velocity gradient $\partial_z u$ over 200 convective time units between the Shercliff layers at $x = 100$ for the UL and QM flow regimes

ACKNOWLEDGMENTS

This work is supported by the Deutsche Forschungsgemeinschaft (DFG) with grants KR 4445/5-1 and SCHU 1410/36-1. The authors also acknowledge the Gauss Center for Supercomputing e.V. (`https://www.gauss-centre.eu`) for providing computing time on the GCS Supercomputer SuperMUC-NG at Leibniz Rechenzentrum (`https://www.lrz.de`) within the computing project ”pn67la”.

REFERENCES

Arlt, T., Priede, J. & Bühler, L. 2017 The effect of finite-conductivity Hartmann walls on the linear stability of Hunt’s flow. *J. Fluid Mech.* **822**, 880–891.

Bejan, A. 2004 *Convection heat transfer, third edition*. John Wiley & Sons.

Braiden, L., Krasnov, D., Molokov, S., Boeck, T. & Bühler, L. 2016 Transition to turbulence in Hunt’s flow in a moderate magnetic field. *Europhys. Lett.* **115** (4), 084501.

Davidson, P. A. 2016 *Introduction to magnetohydrodynamics*. Cambridge University Press.

Krasnov, D., Akhtari, A., Zikanov, O. & Schumacher, J. 2023*a* Tensor-product-Thomas elliptic solver for liquid-metal magnetohydrodynamics. *J. Comp. Phys.* **474**, 111784.

Krasnov, D., Listratov, Ya., Belyaev, I., Kolesnikov, Yu., Sviridov, E. & Zikanov, O. 2023*b* MHD flow of submerged jets behind the inlet disturbance. In *PAMM Proc. Appl. Math. Mech.*, , vol. 22. Wiley-VCH Verlag GmbH & Co. KGaA, Weinheim, special Issue: 92^{nd} Annual Meeting of the International Association of Applied Mathematics and Mechanics (GAMM).

Molokov, S., Moreau, R. & Moffat, H. K. 2007 *Magnetohydrodynamics: Historical Evolution and Trends*. Springer.

Priede, J., Aleksandrova, S. & Molokov, S. 2010 Linear stability of Hunt’s flow. *J. Fluid Mech.* **649**, 115–134.

Smolentsev, S. 2021 Physical Background, Computations and Practical Issues of the Magnetohydrodynamic Pressure Drop in a Fusion Liquid Metal Blanket. *Fluids* **3** (6), 110.

Smolentsev, S., Saedi, S., Malang, S. & Abdou, M. 2013 Numerical study of corrosion of ferritic/martensitic steels in the flowing PbLi with and without a magnetic field. *Journal of Nuclear Materials* **771**, 294–304.